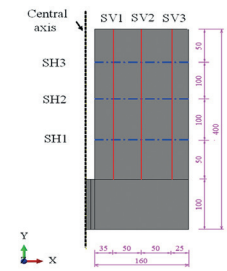


Anchoring performances analysis of tension-torsion grouted anchor under free and non-free rotating conditions

Análisis de las prestaciones de anclaje al terreno bajo solicitaciones de tracción y torsión, en condiciones de rotación libre y coaccionada



■■■■ Shuren Wang^{1,2*}, Yuhao Wang¹, Zeliang Wang¹, Jian Gong¹, and Chunliu Li^{1,3}

¹ International Joint Research Laboratory of Henan Province for Underground Space Development and Disaster Prevention, Henan Polytechnic University, Jiaozuo 454003, China

² Collaborative Innovation Center of Coal Work Safety, Henan Polytechnic University, Jiaozuo 454003, China

³ Institute of Urban Construction, Hebei Normal University of Science & Technology, Qinhuangdao 066004, China

* Corresponding author, e-mail: shurenwang@hpu.edu.cn

DOI: <https://doi.org/10.6036/9985> | Received: 5/sep/2020 • Reviewing: 5/sep/2020 • Accepted: 1/feb/2021

To cite this article: WANG, Shuren; WANG, Yuhao; WANG, Zeliang; GONG, Jian; LI, Chunliu. ANCHORING PERFORMANCES ANALYSIS OF TENSION-TORSION GROUTED ANCHOR UNDER FREE AND NON-FREE ROTATING CONDITIONS. *DYNA*, vol. 96, no 2, p. 166-172. DOI: <https://doi.org/10.6036/9985>

FUNDING

This work was financially supported by the National Natural Science Foundation of China (51774112), and the Fundamental Research Funds for the Universities of Henan Province (NSFRF200202), China.

RESUMEN

- Para el mecanismo de fallo de los recubrimientos del cable de anclaje, en demanda de modelos teóricos, se utilizó una técnica con Abaqus para analizar las prestaciones de anclaje del anclaje inyectado bajo condiciones de rotación libre y coaccionada. Las características del acoplamiento tensión-torsión y el mecanismo de fallo progresivo del segmento de anclaje se estudiaron durante la prueba de extracción. También se analizaron la respuesta a torsión del segmento de anclaje y los cambios internos de deformación horizontal y vertical en el hormigón de anclaje. Los resultados muestran que se verifica el modelo de cálculo propuesto para el cable de anclaje. Con el aumento del desplazamiento de extracción, la respuesta de carga de la sección anclada se transfiere gradualmente desde el interior hacia el exterior. La tensión de anclaje en el hormigón experimenta el proceso de evolución en: "forma de barra" - "forma de campana" - "forma de pecera" - "forma de lanza". Como capa de transición intermedia, el agente de anclaje se romperá antes que el hormigón y, al mismo tiempo, tendrá un efecto amortiguador. Bajo la acción del acoplamiento tensión-torsión, el agente de anclaje es propenso al fallo por tracción y cortante combinado. Hay dos formas diferentes de transmitir la fuerza para el anclaje inyectado en condiciones de rotación y no rotación, y la fuerza de anclaje del cable de anclaje se reducirá en el estado de rotación libre. Las conclusiones obtenidas pueden servir de referencia para una práctica de anclaje similar.
- **Palabras clave:** Anclaje inyectado, Acoplamiento tensión-torsión, Simulación numérica, Mecanismo de fallo, Fuerza de anclaje

ABSTRACT

For the failure mechanism of the anchor cable lags behind the demand for theoretical models, Abaqus technique was used to analyze the anchoring performances of the grouted anchor under the conditions of free and non-free rotating. The tension-torsion

coupling characteristics and the progressive failure mechanism of the anchorage segment were studied during the pull-out test. The torsion response of the anchorage segment and the internal horizontal and vertical strain changes in the anchoring concrete were also analyzed. Results show that the proposed calculation model of the anchor cable is verified. With the increase of the pulling-out displacement, the load response of the anchored section is gradually transferred from the inside to the outside. The anchoring stress in the concrete undergoes the evolution process of rod shape-bell shape-aquarium shape-spear shape. As an intermediate transition layer, the anchoring agent will break before the concrete and at the same time play a buffering effect. Under the action of tension-torsion coupling, the anchoring agent is prone to tensile-shear composite failure. There are two different ways of transmitting force for the grouted anchor under rotating and non-rotating conditions, and the anchoring force of the anchor cable will be reduced in the state of free rotation. The obtained conclusions can provide a reference for the similar anchoring practice.

Keywords: Grouted anchor, Tension-torsion coupling, Numerical simulation, Failure mechanism, Anchoring force.

1. INTRODUCTION

The grouted anchor is usually regarded as an axial linear tension unit [1]. But in fact, it can cause axial displacement and lateral torsion when the grouted anchor is pulled out, and the tension-torsion coupling effect has a great influence on the anchoring force of the grouted anchor.

In recent years, many scholars have paid attention to the shape structure of grouted anchor and the influence on its mechanical properties [2]. Moosavi et al. compared and analyzed three types of special-shaped grouted anchors, and they studied the differences in load transfer and failure modes between the special-shaped and the ordinary grouted anchors [3]. Fan et al. analyzed the influence of the prestressed grouted anchor's geometry on the stress state and failure mechanism of the interface between the grouted anchor and the mortar [4]. Wang et al. studied the mechanical properties of the grouted anchor under the condition of tension-torsion coupling through indoor tensile tests. They proposed the tension-torsion coupling coefficient and defined the percentage of tension used for untwisting of the cable anchor [5].

However, there are few reports on the response characteristics of the anchorage segment of the tension-torsion coupling cable under the conditions of free rotation and non-rotation.

For the current designing method of grouted anchor could not meet the requirement of engineering practice, it is important to propose a reasonable model for the tension-torsion coupling grouted anchor. The model should also be established to reveal the progressive failure mechanism of the anchorage segment in the grouted anchor under the conditions of free rotation and non-rotation. It is of great theoretical significance and practical value for deepening the anchoring mechanism of the tension-torsion coupling grouted anchors.

2. STATE OF THE ART

Since the 1990s, some scholars have carried out a large number of relevant studies and put forward different forms of bond-slip models for the grouted anchor. For examples, Malvar proposed the famous malvar model in 1994 [6]. Benmokrane et al. proposed a tri-linear model to reflect the interfacial shear slip relationship between the anchorage and the surrounding rock in 1995 [7]. Consenza et al. proposed the modified Bertero-Popov-Eligehausen (BPE) model in 1996 [8]. Recently, Ren et al. derived the axial stress distribution of the anchor along the anchoring length based on a tri-linear model with residual bond strength [9], and the related research works [10-16].

For the numerical simulation of anchoring effect, Zhao et al. used the Cohesive Zone Model (CZM) to simulate the fiber pull-out from the matrix, crack propagation and interface failure [17]. Xu et al. carried out the research on the anchoring mechanism of the prestressed anchor rod in the fractured rock mass by using different rod elements for the grouted anchor [18]. Chen et al. proposed the three-dimension elasto-viscoplastic composite element considering the viscoplastic properties of materials to simulate the pull-out slip deformation and failure of the fully grouted rock bolts [19]. Chen et al. simulated the pull-out behavior of the ordinary and the improved grouted anchors, and they analyzed the restraint effect of the passive constraint medium on the two kinds of grouted anchors [20]. Deb and Das simulated and analyzed the mechanical properties of the rock mass reinforced by the fully grouted rock bolts [21]. Nemcik et al. used a non-linear bond-slip model to simulate the axial response of the fully grouted rock anchors [22]. Yokota et al. studied the interface behavior between the rock bolts and the bonding material, as well as the crack initiation and propagation inside the bond material, and they assessed the influence of the ribs and rib angle of the anchor rod, the strength of the bond material and the confining pressure on the anchorage [23].

Though most scholars focus on the simulation and analysis of the tensile performance of the anchoring elements under pull-out loading, while the response characteristics of the anchoring units of the grouted anchor under the tension-torsion coupling condition are often ignored [24-26]. Therefore, taking the grouted anchor as the research object, the computational model of the grouted anchor was established based on the tension-torsion coupling effect of the anchorage segment. The spatial and temporal distribution characteristics of stress and strain in the anchoring concrete, the transmitting force for the grouted anchor under rotating and non-rotating conditions and the progressive failure mechanism of the anchorage segment will be studied during the pulling-out test. The research results can provide a reference for the similar engineering practice.

The rest of this study is organized as follows. In Section 3, the numerical calculation model of the tension-torsion coupling grouted anchor is established. Section 4 makes a comprehensive analysis of the calculated results to reveal the mechanical response of the anchorage segment of the grouted anchor under rotating and non-rotating conditions. Finally, some conclusions are summarized in Section 5.

3. METHODOLOGY

3.1. THE COMPUTATIONAL MODEL

The calculation model is shown in Fig. 1. For the tension-torsion coupling effect, the established calculation model of the grouted anchor should follow such assumptions being made: (1) The material of the model is homogeneous, continuous and isotropic; (2) The influence of time on the material properties is not considered; (3) The interface between the anchoring agent and the concrete fits well without relative slip.

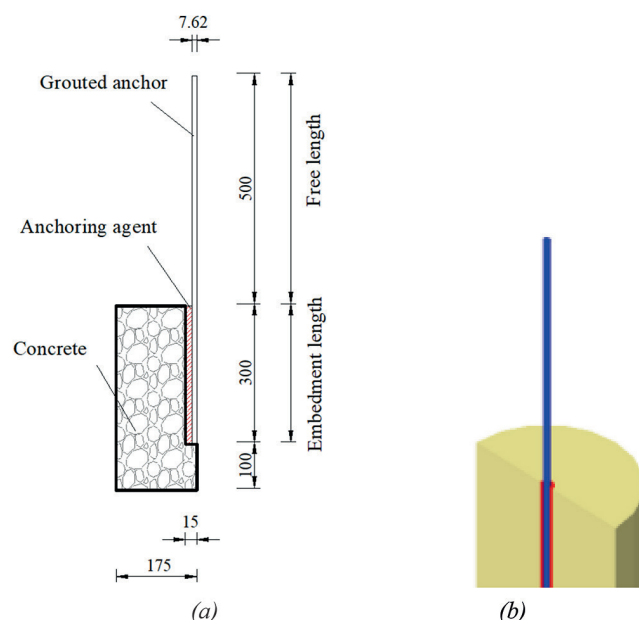


Fig. 1. The computational model and its section size (mm). (a) Section size of the model; (b) The simulation model

There are usually three main modelling methods: separated, combined and integrated. In this study, the separate modelling is method adopted. The numerical model consists of grouted anchor, anchoring agent, concrete and the baffle. Setting the baffle on the top of the concrete is used to simulate the lower transverse beam (the bearing plate or reaction frame commonly used in the pull-out test) of the grouted anchor tension-torsion coupling testing machine, which is a simplification of the physical test model. The concrete and anchoring agent are set into a complete structure in the model, and the two types structural units share the same node to transfer the force and displacement through the dissection elements.

Considering the structure and load characteristics of the model, the calculation model is carried out according to the axisymmetric problem to reduce the calculation cost. The anchorage section and anchoring agent are used as the main contact area, and the meshes of the model are shown in Fig. 2 (See section: supplementary material). The element shape is quad and the grid algo-

rithm is medial axis. The grouted anchor has 3500 units, concrete and anchoring agent total have 11820 units. For the force transferring characteristics of the grouted anchor, the CGAX element in Abaqus is used to simulate the structural response of the grouted anchor under the conditions of free rotation and non-rotation.

3.2. MATERIALS AND INTERFACE PARAMETERS

The mechanical parameters of three materials (grouted anchor, anchoring agent and concrete) used in the model are listed in Tables I, II, and III (See section: supplementary material).

The Concrete Damaged Plasticity (CDP) model [27] in Abaqus and the stress-strain relationships of uniaxial compression and tension recommended in China Code for design of concrete structures (GB 50010-2010) are used to simulate the mechanical response of concrete under the tension-torsion condition, the stress-strain curves of uniaxial compression and tensile of concrete are shown in Fig. 3 (See section: supplementary material) [28]. The parameters of CDP model are listed in Table IV.

Name	Ψ (°)	ϵ	α_f	K_c	μ
Value	38	0.1	1.16	0.66667	0.00001
Note	Ψ is the dilation angle. ϵ is the flow potential offset. α_f is the ratio of biaxial compressive strength to uniaxial compressive strength. K_c is the ratio of the second invariant stress on the meridian in tension and the meridian in compression. μ is the viscosity coefficient.				

Table IV. The parameters of CDP model

Considering that the grouted anchor is within the limit strength, the ideal elastic-plastic model is utilized for the grouted anchor. The curve of the stress-strain relationship of grouted anchor is shown in Fig. 4 (See section: supplementary material) [29].

The surface-based cohesive behavior in the Abaqus/Standard and the quadratic stress criterion are used to simulate the bond and peel behaviors at the interface between the grouted anchor and the anchoring agent, the typical traction - separation response is shown in Fig.5 (See section: supplementary material) [30].

There are four criteria for starting damage: maximum stress criterion, maximum separation criterion, quadratic stress criterion, and quadratic separation criterion. The quadratic stress criterion is adopted (formula 1) [30].

$$\left(\frac{t_n}{t_n^{max}}\right)^2 + \left(\frac{t_s}{t_s^{max}}\right)^2 + \left(\frac{t_t}{t_t^{max}}\right)^2 = 1 \quad (1)$$

In the formula, the t_n is the normal contact stress in pure normal mode, the t_s is the shear contact stress along the first shear direction, and the t_t is the shear contact stress along the second shear direction. The t_n^{max} is the maximum normal contact stress in pure normal mode, the t_s^{max} is the maximum shear contact stress along the first shear direction, and the t_t^{max} is the maximum shear contact stress along the second shear direction.

The peak value of pull-out load is measured by the pull-out test [5], and then the bond stress is calculated as the bond strength of the interface, so the following formula can be used [31]:

$$\tau = \frac{F}{\pi dl} \quad (2)$$

where, τ is the bond strength, F is the peak value of the pull-out load, d is the diameter of the grouted anchor, and l is the embedment length.

The CZM has three independent directions in the space, Yang and Thouless proposed that mode II crack parameters play a dominant role in the process of interface fracture failure, and the parameters of mode I crack and mode II can be taken as the same value [32]. The parameters of the interface stiffness and peak stress are listed in Table V (See section: supplementary material).

The damage evolution is based on the pull-out displacement and it is in exponential form. The viscosity coefficient is 0.00001 in the viscosity regularization based on the viscous behavior of the surface. When the bond fails, the normal behaviour is "hard" contact, the tangential behaviour is "penalty", and the friction coefficient is 0.3.

3.3. LOADING MODE AND BOUNDARY CONDITIONS

In the study, Abaqus/Standard is used as the solver, and the analysis step type is set to Static, The numerical model adopts the displacement loading mode, which is divided into three analytical steps. The curve of the displacement-analysis step time is shown in Fig. 6 (See section: supplementary material).

The boundary conditions of SBZ and SZ are shown in Fig. 7 (See section: supplementary material) (SBZ means that the free end of the grouted anchor is fixed and it does not rotate, and the freedom degree of rotating along the axial direction is in the constrained state. SZ means that the free end of the grouted anchor is free and it can rotate, and the freedom degree of rotating along the axial direction is in the open state). In these two models, the free end of the grouted anchor is subject to the upward pull-out load, and the anchorage end has torsion along the axial direction. A reference point is defined at the right end of the baffle, which is set as the fully fixed to constrain all degrees of freedom of the baffle. The upper boundary of the concrete contacts with the baffle, and the "frictionless" contact is adopted between the concrete and the baffle. The lower boundary of concrete is fully constrained. The concrete is subjected to the confining pressure of 5.0 MPa in the radial direction.

4. RESULT ANALYSIS AND DISCUSSION

4.1. VALIDATION OF THE COMPUTATIONAL MODEL

Based on the characteristic curves of the axial tension and torque obtained from the indoor pull-out loading test for the grouted anchor, the tension-torsion coupling calculation model

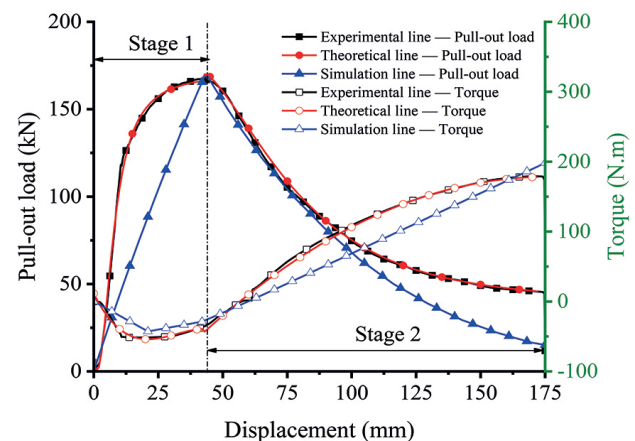


Fig. 8. Comparison of experimental, theoretical and simulation results

was proposed. To verify the rationality of the calculation model, the curves of the experimental, the theory and the simulation were compared and analyzed. As shown in Fig. 8, the changing trends of the three curves are basically the same, and the rationality of the parameter setting of the calculation model is checked, which provides a calculation basis for the numerical simulation of the tension-torsion coupling effect of the grouted anchor.

To verify the shear stress of anchorage agent under peak axial tension on the interface between grouted anchor and anchorage agent, monitor line "GL" is arranged on the left side of anchorage agent on the contact surface between grouted anchor and concrete, as shown in Fig. 9 (See section: supplementary material). The "GL" represents the interface between grouted anchor and anchorage agent.

It should be clearly pointed out that the "distance" of the abscissa in the data Fig. 9 (See section: supplementary material) is the distance between the grid nodes picked up along the route from the starting point to the end point in a certain direction.

The curves of shear stress S_{12} distribution of anchorage agent at the interface between grouted anchor and anchorage agent are shown in Fig. 10 (See section: supplementary material). The "GL" base on the lower boundary of anchorage agent, from bottom to top, the distance of each node is 0-300 mm from the lower boundary.

Fig. 10 (See section: supplementary material) shows that the shear stress under SBZ state is 13.14 MPa and that under SZ state is 10.53 MPa. The accuracy of the model and parameters is confirmed again by the K_{nn} , K_{ss} and K_{tt} are 13.70 MPa, t_n^{\max} , t_s^{\max} and t_t^{\max} are 10.57 MPa in Table V (See section: supplementary material), respectively.

4.2. CHARACTERISTICS OF TENSION-TORSION COUPLING

To vividly describe the evolution process of each anchorage unit from the beginning of loading to the failure of anchorage within the system, and to reflect the loading stage (stage 1) and softening stage (stage 2) in the tension-torsion coupling model, the load transferring characteristics of the grouted anchor under the conditions of free rotation and non-rotation was analyzed. As shown in Fig. 11, the evolution process of the anchoring stress of the non-rotation grouted anchor was selected by using the sweep function of the post-processing in Abaqus.

It can be seen from Fig. 11. under the condition of non-rotation, the load transferring path of the grouted anchor is: first from the free section of the grouted anchor to the anchorage segment. With the increase of the analysis step time, the load transferring of the anchoring system changes from the grouted anchor to the anchorage agent, then turn to the concrete, and gradually presents the evolution process of rod shape–bell shape–aquarium shape–spear shape from the inside to the outside.

Loading stage (stage 1): when $t = 0-0.014$ s, the free section of the grouted anchor is stressed first (Figs. 4(a) to 4(b)). When $t = 0.014-0.050$ s, the load is transferred from the free section to the anchorage segment after the free section being filled (Figs. 4(b) to 4(e)). When $t = 0.172$ s, the load penetrates from the upper and lower ends of the anchoring agent to the middle (Fig. 4(f)), forming a weak "rod shape". When $t = 0.559-0.759$ s, the stress of the anchoring stress gradually expands from the inside to the outside, and the shape of the anchoring stress gradually presents a "bell shape" (Figs. 4(g) to 4(h)). When $t = 0.959-2$ s, with the continuous increase of the pulling force of the grouted anchor, the influence range of the anchoring stress gradually becomes larger, and the stress pattern in the concrete changes from "bell shape"

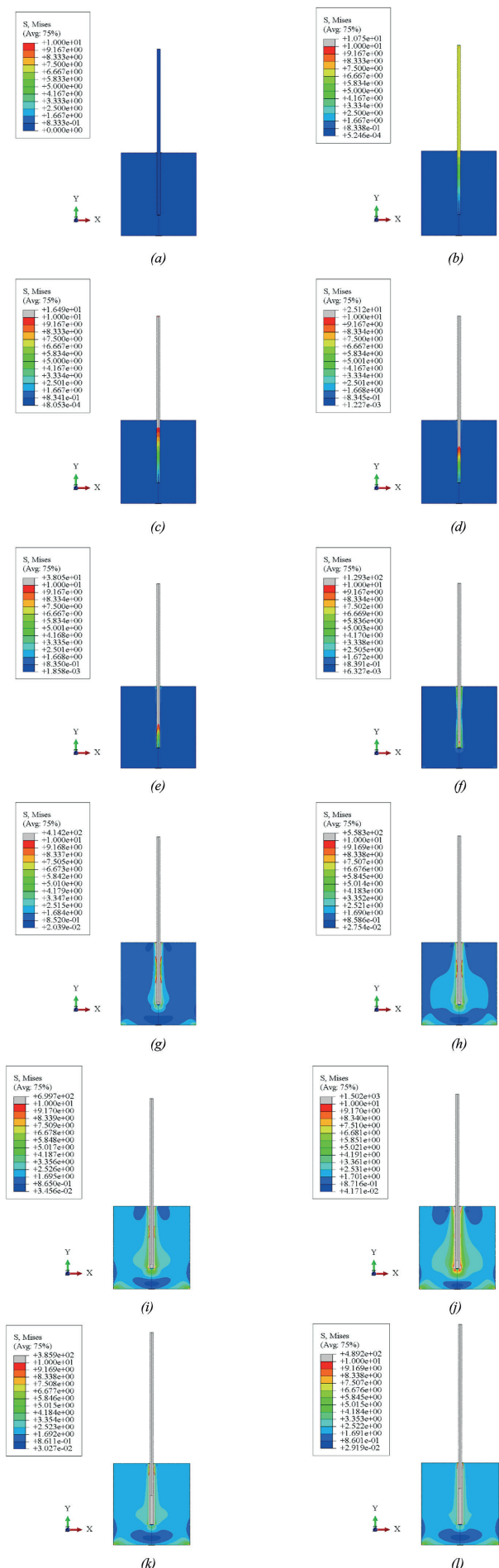


Fig. 11. Anchoring stress evolution in the anchoring system (unit: MPa). (a) $t=0$ s; (b) $t=0.014$ s; (c) $t=0.022$ s; (d) $t=0.033$ s; (e) $t=0.050$ s; (f) $t=0.172$ s; (g) $t=0.559$ s; (h) $t=0.759$ s; (i) $t=0.959$ s; (j) $t=2$ s; (k) $t=2.759$ s; (l) $t=3$ s

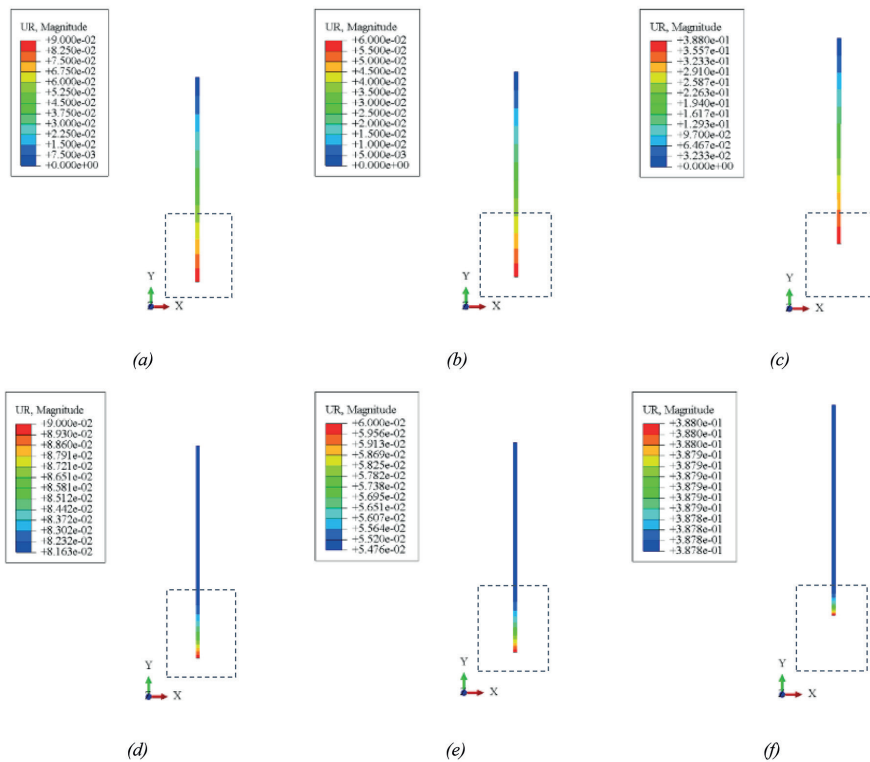


Fig. 12. Torsion angles of grouted anchor (unit: rad). (a) SBZ model $t = 1$ s; (b) SBZ model $t = 2$ s; (c) SBZ model $t = 3$ s; (d) SZ model $t = 1$ s; (e) SZ model $t = 2$ s; (f) SZ model $t = 3$ s

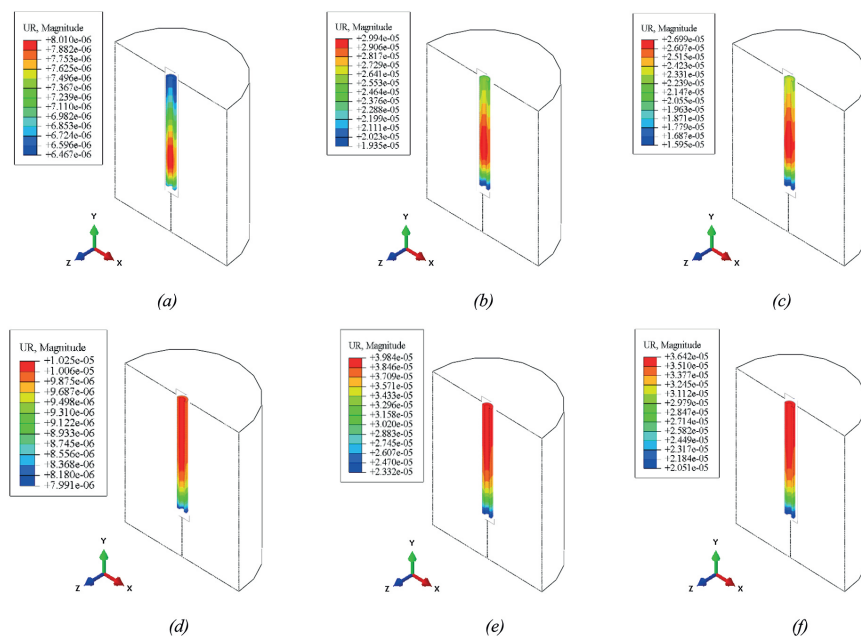


Fig. 13. Torsion angle of anchoring agent (unit: rad). (a) SBZ model $t = 1$ s; (b) SBZ model $t = 2$ s; (c) SBZ model $t = 3$ s; (d) SZ model $t = 1$ s; (e) SZ model $t = 2$ s; (f) SZ model $t = 3$ s

to "aquarium shape", and the stress growth period is stable (Figs. 4(i) to 4(j)).

Softening stage (stage 2): As shown in Figs. 4(j) to 4(l), when $t = 2-3$ s, when the pull-out load reaches the limit value, the anchoring stress also reaches the peak value. With the increase of the pull-out displacement of the grouted anchor, the anchoring stress of the anchor begins to fluctuate and decay, and enters the stress decline period. The stress pattern in the concrete gradually decays from "aquarium shape" to "spear shape".

4.3. ANALYSIS OF TORSIONAL RESPONSE CHARACTERISTICS

4.3.1. Torsional response characteristics of grouted anchor

The torsion state reflects the rotation deformation of the grouted anchor under the tension-torsion coupling effect. The change process of torsion angle of the grouted anchor under different analytical step time is shown in Fig. 12.

It can be seen from Figs. 12(a) to 12(c) and 12(d) to 12(f), the torsion angle of the lowest end of the grouted anchor is basically the same in both cases. It shows that under the influence of the anchoring interface, the grouted anchors have the torque actively applied along the clockwise direction, and then rotate from the bottom to top, but torsional response of the grouted anchor is different because of the different constraint state at the top of the grouted anchor.

It can be seen from Figs. 12(a), 12(b), and 12(c), under the SBZ state, the torsion distribution of the grouted anchor is uneven, and the torsion is mainly concentrated in the middle and lower segments of the grouted anchor, and it gradually decreases from the bottom to top, and the torsion angle at the top end is 0.

On the other hand, as seen from Figs. 12(d), 12(e), and 12(f), under the SZ state, the torsion distribution of the grouted anchor is relatively uniform, and the torsion angle at the lower end is the largest. The internal torsion angle of grouted anchor decreases from the bottom to top, but the change range are small.

4.3.2. Torsional response characteristics of anchoring agent

The torsion angle of anchoring agent is shown in Fig. 6. What can be seen from Figs. 6(a) and 6(b) (See section: supplementary material) is that, the rotation states of the two anchoring agents are different, which results in the failure location and damage history of the anchoring agent.

It can be seen from Figs. 13(a) to 13(c), under the SBZ state, the torsion distribution of the anchoring agent is relatively uneven, and the torsion angle of the middle and lower parts is larger, but the concentration range is not large. The torsion failure will start from the lower part of the anchorage segment, and then gradually transfer to the middle part of the anchorage segment when the anchoring agent in the lower part is completely destroyed, and the development process is slow, thus the tensile-shear failure occurs.

As seen from Figs. 13(d) to 13(f), under SZ state, the torsion distribution of anchoring agent is relatively uniform, and the rotation is mainly concentrated in the middle and upper part of the

anchorage segment, and the concentration range is large. The torsion failure starts from the upper part of the anchorage segment, which is prone to failure under the end effect, and then extends to the middle of the anchorage segment along the fracture. The torsion angle of SZ state is larger than that of the SBZ state. Under the action of large shear stress and shear range, the debonding and peeling speed of the anchoring agent and grouted anchor interface is faster, so the anchoring force is reduced.

4.4. VARIATION CHARACTERISTICS ANALYSIS OF STRAIN

To obtain the strain variation characteristics in the anchoring concrete under the maximum pull-out load, the monitoring lines are set as shown in Fig. 14. The horizontal monitoring line is based on the left boundary of the anchoring concrete, and the distance range is 0–160 mm. The vertical monitoring line is based on the lower boundary of the anchoring concrete with a distance of 100–400 mm.

As shown in Fig. 15, under SBZ and SZ states, the horizontal and vertical strain distributions of the anchorage segment in the anchoring concrete are similar. This is because that the anchoring agent is the grouting body. As the intermediate transition layer, it is the link between the grouted anchor and the concrete. In the process of pull-out loading, the anchoring agent not only plays the role of connecting the anchoring unit, but also consumes energy in the process of load transferring, which makes the internal force of itself increase and the anchoring agent will be destroyed before the concrete. At the same time, it also plays a buffer role. Especially for the torsion, the energy consumption effect is more significant. However, the overall strain value of SBZ is greater than that of SZ, which indicates that the ability of SBZ to mobilize concrete is stronger than that of SZ, and it can play a better role in anchoring.

It can be seen from Fig. 15(a), the horizontal strain increases first and then decreases from the inside to the outside in the an-

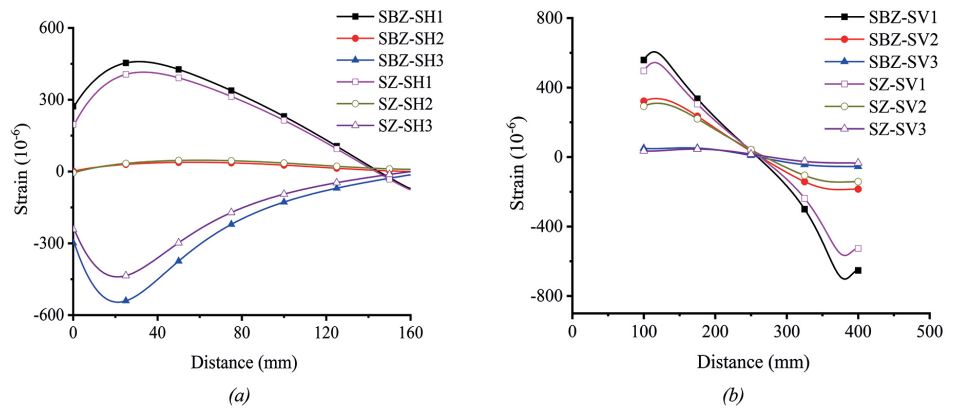


Fig. 15. The strain distribution curves of the monitoring lines. (a) The horizontal line; (b) The vertical lines

choring concrete, and finally tends to 0 at the far end from the central axis. The strain distribution of SH1 and SH3 with respect to SH2 is upper and lower symmetric, and both have concavity and convexity.

As can be seen from Fig. 15(b), the overall vertical strain from the bottom to the top takes the strain at 250 mm away from the lower boundary of the anchoring concrete as the central point, which is symmetrically distributed in the center, showing opposite tension and compression regions.

5. CONCLUSIONS

To reveal the failure mechanism of the grouted anchor, Abaqus technique was used to analyze the anchoring performances of the grouted anchor under the conditions of free rotation and non-rotation. The main conclusions are as following:

- (1) The calculation model for the tension-torsion coupling grouted anchor is proposed and its rationality is verified. With the increase of the pull-out displacement, the load transferring process of the anchorage segment gradually diffuses from the inside to the outside of the anchoring concrete, and experiences the process evolution of rod shape–bell shape–aquarium shape–spear shape.
- (2) The restraint condition of the free end of the grouted anchor affects the torsional shape and force transferring mode of the anchorage system, which makes the torsional response position different. The torsional response has great influence on the anchoring agent, but which has a little effect on the concrete. As an intermediate transition layer, the anchoring agent plays a buffer role in the process of the load transferring.
- (3) The horizontal and vertical strain changes in the anchoring concrete under the condition of non-rotation and free rotation states are basically the same. However, under the non-rotation state, the anchorage system of the grouted anchor can provide greater pull-out load and plays a better anchoring effect.

In the research project (51774112), the anchorage segment is not only subjected to the medium and high confining pressure, but also subjected to the shear, torsion and dynamic impact. In the future, the transparent similar materials will be used to carry out the tensile and torsional test of the anchorage segment under the combined loading of shear, torsion and dynamic impact.

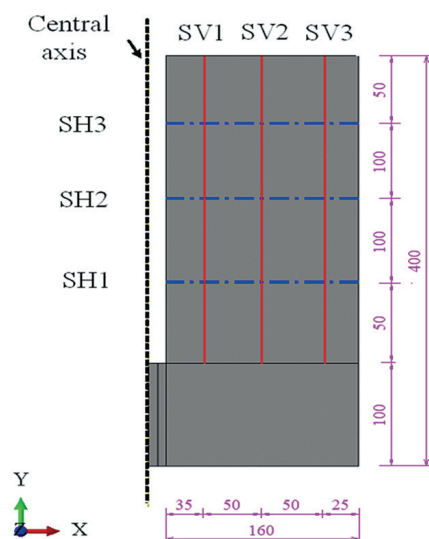


Fig. 14. The layout of monitoring lines in the anchoring concrete

REFERENCES

- [1] Francisca B, Ben L, Jeff W. "Deadman anchoring design for cable logging: A new approach". *Canadian Journal of Forest Research*. December 2019. Vol. 50-3. p. 342-357. DOI: <https://doi.org/10.1139/cjfr-2019-0338>
- [2] Wang SR, Xiao HG, Zou ZS, Cao C, Wang YH, Wang ZL. "Mechanical performances of transverse rib bar during pull-out test". *International Journal of Applied Mechanics*. June 2019. Vol. 11-5. p. Article ID 1950048: 1-15. DOI: <https://doi.org/10.1142/S1758825119500480>
- [3] Moosavi M, Bawden WF, Hyett AJ. "Mechanism of bond failure and load distribution along fully grouted cable-bolts". *Mining Technology*, April 2002. Vol. 111-1. p. 1-12. DOI: <https://doi.org/10.1179/mnt.2002.111.1.1>
- [4] Fan YJ, Zheng QZ, Wei L. "Research on failure mechanism and ultimate load carrying capacity of prestressed cable". *Chinese Journal of Rock Mechanics and Engineering*. August 2005. Vol. 24-15. p. 2765-2769. DOI: <https://doi.org/10.3321/j.issn:1000-6915.2005.15.028>
- [5] Wang SR, Wang YH, Gong J, Wang ZL, Huang QX, Kong FL. "Failure mechanism and constitutive relation for an anchorage segment of an anchor cable under pull-out loading". *Acta Mechanica*. August 2020. Vol. 231-8. p. 3305-3317. DOI: <https://doi.org/10.1007/s00707-020-02717-4>
- [6] Malvar LJ. "Tensile and bond properties of GFRP reinforcing bars". *ACI Materials Journal*. May 1995. Vol. 93-3. p. 276-285. DOI: [https://doi.org/10.1016/0040-6090\(94\)06475-X](https://doi.org/10.1016/0040-6090(94)06475-X)
- [7] Benmokrane B, Chennouf A, Mitri HS. "Laboratory evaluation of cement-based grouts and grouted rock anchors." *International Journal of Rock Mechanics and Mining Sciences and Geomechanics Abstracts*. October 1995. Vol. 32-7. p. 633-642. DOI: [https://doi.org/10.1016/0148-9062\(95\)00021-8](https://doi.org/10.1016/0148-9062(95)00021-8)
- [8] Cosenza E, Manfredi G, Realforzo R. "Behavior and modeling of bond of FRP rebars to concrete". *Journal of Composites for Construction*. May 1997. Vol. 1-2. p. 40-51. DOI: [https://doi.org/10.1061/\(ASCE\)1090-0268\(1997\)1:2\(40\)](https://doi.org/10.1061/(ASCE)1090-0268(1997)1:2(40))
- [9] Ren FF, Yang ZJ, Chen JF, Chen WW. "An analytical analysis of the full-range behaviour of grouted rockbolts based on a tri-linear bond-slip model". *Construction and Building Materials*. March 2010. Vol. 24-3. p. 361-370. DOI: <https://doi.org/10.1016/j.conbuildmat.2009.08.021>
- [10] Bilić Z, Samardžić I, Mišina N, Stoić K. "Preliminary research on influence of welding parameters strength at welded joints in ribbed reinforcing steel". *Technical Journal*. September 2020. Vol. 14-3. p. 369-374. DOI: <https://doi.org/10.31803/tg-20200303111417>
- [11] Krantovska O, Petrov M, Ksonshkevych L, Orešković M, Synii S, Ismailova N. "Numerical simulation of the stress-strain state of complex-reinforced elements". *Technical Journal*. June 2019. Vol. 13-2. p. 110-115. DOI: <https://doi.org/10.31803/tg-20190417112619>
- [12] Li Z, Zhou H, Hu DW, Zhang CQ. "Yield criterion for rocklike geomaterials based on strain energy and CMP model". *International Journal of Geomechanics*. March 2020. Vol. 20-3. p. Article ID 04020013: 1-13. DOI: [https://doi.org/10.1061/\(ASCE\)GM.1943-5622.0001593](https://doi.org/10.1061/(ASCE)GM.1943-5622.0001593)
- [13] Yan MJ, Xia YY, Liu TT, Bowa VM. "Limit analysis under seismic conditions of a slope reinforced with prestressed anchor cables". *Computers and Geotechnics*. April 2019. Vol. 108. p. 226-233. DOI: <https://doi.org/10.1016/j.compgeo.2018.12.027>
- [14] Robert S, Michal T, Stanislav K. "Analysis of wind-induced vibrations of an anchor cable using a simplified fluid-structure interaction method". *Applied Mathematics and Computation*. September 2015. Vol. 267. p. 223-236. DOI: <https://doi.org/10.1016/j.amc.2015.03.114>
- [15] Xiang YQ, Chen ZY, Yang Y, Lin H, Zhu S. "Dynamic response analysis for submerged floating tunnel with anchor-cables subjected to sudden cable breakage". *Marine Structures*. May 2018. Vol. 59. p. 179-191. DOI: <https://doi.org/10.1016/j.marstruc.2018.01.009>
- [16] Xu LZ, Wei SJ. "Control technology and simulation study of floor heave in high stress soft rock roadway". *Geotechnical and Geological Engineering*. August 2020. Vol. 38-4. p. 4045-4058. DOI: <https://doi.org/10.1007/s10706-020-01276-8>
- [17] Zhao YP, Yuan H, Han J. "Analysis of the macroscopic interfacial behaviour of the fibre pullout using elastic-plastic cohesive model". *Chinese Journal of Theoretical and Applied Mechanics*. January 2015. Vol. 47-1. p. 127-134. DOI: <https://doi.org/10.6052/0459-1879-14-165>
- [18] Xu QW, You CA, Zhu HH. "Study on 3D numerical simulation of prestressed anchor cable and its application". *Chinese Journal of Rock Mechanics and Engineering*. July 2004. Vol. 23-7. p. 4942-4945. DOI: <https://doi.org/10.3321/j.issn:1000-6915.2004.7.048>
- [19] Chen SH, Qiang S, Chen SF, Egger P. "Composite Element Model of the Fully Grouted Rock Bolt". *Rock Mechanics & Rock Engineering*. July 2004. Vol. 37-3. p. 193-212. DOI: <https://doi.org/10.1007/s00603-003-0006-z>
- [20] Chen J, Saydam S, Hagan PC. "Numerical simulation of the pull-out behaviour of fully grouted cable bolts". *Construction and Building Materials*. December 2018. Vol. 191. p. 1148-1158. DOI: <https://doi.org/10.1016/j.conbuildmat.2018.10.083>
- [21] Deb D, Das KC. "Modelling of fully grouted rock bolt based on enriched finite element method". *International Journal of Rock Mechanics & Mining Sciences*. February 2011. Vol. 48-2. p. 283-293. DOI: <https://doi.org/10.1016/j.ijrmms.2010.11.015>
- [22] Nemcik J, Ma SQ, Aziz N, Ren TX, Gen XY. "Numerical modelling of failure propagation in fully grouted rock bolts subjected to tensile load". *International Journal of Rock Mechanics & Mining Sciences*. October 2014. Vol. 71. p. 293-300. DOI: <https://doi.org/10.1016/j.ijrmms.2014.07.007>
- [23] Yokota Y, Zhao ZY, Nie W, Date K, Iwano K, Okada Y. "Experimental and numerical study on the interface behaviour between the rock bolt and bond material". *Rock Mechanics and Rock Engineering*. March 2019. Vol. 53-3. p. 869-879. DOI: <https://doi.org/10.1007/s00603-018-1629-4>
- [24] Li HC, Ding K, Xu Q, Zhang Q. "Mechanism of coordinate anchorage support of bolt-single anchor cable for gob-side entry roof". *Geotechnical and Geological Engineering*. April 2019. Vol. 37-2. p. 857-867. DOI: <https://doi.org/10.1007/s10706-018-0656-y>
- [25] Kim JH, Song CY. "Evaluation of anchor pile penetration characteristics according to soil type to ensure burial safety of subsea cable". *Transactions of the Korean Society of Mechanical Engineers, A*. May 2020. Vol. 44-5. p. 369-375. DOI: <https://doi.org/10.3795/KSME-A.2020.44.5.369>
- [26] Rasoul A, Karim A, Reza CM. "Investigation into pre-stress modes and optimal layout of a new hybrid cable-strut system". *Advances in Structural Engineering*. May 2020. Vol. 23-7. p. 1259-1275. DOI: <https://doi.org/10.1177/1369433219891798>
- [27] Lubliner J, Oliver J, Oller J, Onate E. "A plastic-damage model for concrete". *International Journal of Solids & Structures*. December 1989. Vol. 25-3. p. 299-326. DOI: [https://doi.org/10.1016/0020-7683\(89\)90050-4](https://doi.org/10.1016/0020-7683(89)90050-4)
- [28] Baniasad E, Dehestani M. "Incorporation of corrosion and bond-slip effects in properties of reinforcing element embedded in concrete beams". *Structures*. August 2019. Vol. 20. p. 105-115. DOI: <https://doi.org/10.1016/j.istruc.2019.03.004>
- [29] Wang YJ, Wu ZM, Zheng JJ, Yu RC, Liu Y. "Analytical method for crack propagation process of lightly reinforced concrete beams considering bond-slip behaviour". *Engineering Fracture Mechanics*. October 2019. Vol. 220-15. p. Article ID 106654: 1-16. DOI: <https://doi.org/10.1016/j.engfracmech.2019.106654>
- [30] Chen ZH, Wei C, Luo QW, Di J. "Analysis on mechanical properties of FRP retrofitted concrete beam-column structure using cohesive model". *Journal of Building Structures*. September 2019. Vol. 40-9. p. 122-130. DOI: <https://doi.org/10.14006/j.jzjgxb.2017.0505>
- [31] Ma S, Nemcik J, Aziz N. "Simulation of fully grouted rockbolts in underground roadways using FLAC2D". *Canadian Geotechnical Journal*. December 2014. Vol. 51-8. p. 911-920. DOI: <https://doi.org/10.1139/cgj-2013-0338>
- [32] Yang QD, Thouless MD. "Mixed-mode fracture analysis of plastically-deformation adhesive joints". *International Journal of Fracture*. July 2001. Vol. 110-2. p. 175-187. DOI: <https://doi.org/10.1023/A:1010869706996>

SUPPLEMENTARY MATERIAL

https://www.revistadyna.com/documentos/pdfs/_adic/9985-1.pdf

